RF METROLOGY OF LUNAR HIGHLANDS REGOLITH SIMULANT NU-LHT-2M

Kerry J. Johnson, Elise M. Eckman, Aaron J. Swank, Michael J. Zemba
NASA Glenn Research Center, 21000 Brookpark Rd, Cleveland, OH

Abstract

Understanding the electrical properties of lunar regolith is vital to modeling radiofrequency (RF) propagation on the lunar surface, a fundamental step in planning lunar surface missions. Near the lunar south pole, the regolith has yet to be directly sampled and thus there remains uncertainty in the electrical properties of the regolith. The regolith simulant NU-LHT-2M is a highlands simulant that is representative of the expected chemical composition of the regolith near the lunar south pole. Previous studies have investigated properties of NU-LHT at UHF and S-band[1]. Future missions to the lunar south pole are expected to utilize X and Ka-band for direct-to-Earth links and UHF, S-band, C-band, and Ka-band for lunar surface communication [2]. As a result, it is necessary to electrically characterize the lunar regolith at these frequencies. In this paper, coaxial impedance dielectric reflectometry is performed on the NU-LHT-2M simulant using a commercially available soil permittivity measurement device. This study serves as a preliminary measurement of the simulant and may lead to enhanced efficacy of the measurement hardware for future applications.

Introduction

Understanding the electrical properties of lunar regolith is vital to modelling the RF propagation channel for the design of lunar communications links. Currently, there is significant interest in exploring the lunar south pole, a region of the moon where the regolith has yet to be directly measured or sampled and where the electrical properties are thus not fully characterized. Since the RF communication links at the lunar south pole (surface-to-surface as well as direct-to-Earth) will face very low elevation angles with grazing paths along the terrain, the impact of the terrain is non-negligible on both surface-to-surface and surface-to-Earth links and accurate models of the regolith are necessary. In the absence of in-situ measurements, RF characterization of lunar regolith simulants with chemical compositions similar to the south pole provides an opportunity to improve estimates of the regional electrical properties. By improving estimates for RF characteristics, the fidelity of propagation models for communication links is enhanced, and the overall mission safety is improved by building confidence in pre-flight simulations, emulation, and testing.

The regolith simulant NU-LHT-2M is a highlands simulant that is expected to have chemical compositional similarity to the lunar south pole. Future missions to the lunar south pole, both crewed and robotic, will utilize communication links at X and Ka-band for direct to Earth and UHF, S-, C-, and Ka-band for lunar surface communications [2], so these bands are of the most relevance for regolith metrology. In this paper, the Stevens HydraProbe soil sensor is used for coaxial impedance dielectric reflectometry of the NU-LHT-2M sample. This study serves as a preliminary evaluation of the instrument for regolith simulant characterization, which may lead to enhanced efficacy of the probe for future simulant characterization efforts as well as in-situ usage for field testing lunar communications systems.

The regolith simulant NU-LHT-2M (NASA/USGS-Lunar Highlands type) is based on the average chemical composition of samples from Apollo 16's landing in the moon's Descartes Highlands (8.9730 °S, 15.5002 °E) [3]. The simulant (shown in Figure 1) is "made from a combination of Stillwater Norite, Anorthosite, and Hartzburgite, and Twin Sisters Dunite; partially and fully melted Stillwater mill waste was added as 'pseudo-agglutinates' and 'good glass', respectively. The -2M version also includes natural ilmenite, synthetic whitlockite, natural fluor-apatite, and natural pyrite" [4]. Table 1 provides the chemical composition of the LHT prototype. The -2M simulant variant compositionally contains crystalline, agglutinate, & good glass percentage breakdowns of 65%, 30%, and 5%, respectively [3].

Table 1. Chemical composition of a prototype for the lunar highland simulant [3]

Oxide:	**SiO_2**	**Al_2O_3**	**FeO**	**MgO**	**CaO**	**Na_2O**
Weight %	47.6	24.4	4.3	8.5	13.1	1.4

Figure 1: Sample of lunar highlands regolith simulant LHT-2M

The particle size distribution of the simulant was tested rigorously and selected to track the Apollo results very closely [4]; the resultant simulant particle size distribution falls within one standard deviation of lunar sample characteristics. This similarity is valuable as the dielectric properties of the terrain can vary with the size and composition of the constituent regolith particles. The particle size distribution of a particular region can affect the overall density and homogeneity of the individual dielectrics composing the regolith. Finer particles may have different dielectric properties than coarser particles, affecting how they interact with microwaves as a bulk substrate. The more non-uniform the powder species is, the higher the likelihood of observing significant variations in the propagation characteristics over different regions when modeling communications links.

Methodology

The dielectric properties of a material, such as its permittivity and loss tangent, affect its RF transmission and reflection. Electrical characteristics of a material are described by the dielectric constant, K, permittivity, ε, and conductivity, σ. The dielectric constant is related to the complex permittivity, defined relative to values at vacuum:

$$K = \frac{\varepsilon}{\varepsilon_0} = \varepsilon_r = \varepsilon_r' - j\,\varepsilon_r'' = \frac{\varepsilon_r'}{\varepsilon_0} - j\frac{\sigma}{\omega\varepsilon_0}$$

where the real and imaginary parts of the complex relative permittivity, ε_r are given by ε_r' and ε_r'', respectively. The vacuum permittivity is given by ε_0 and ω is the radial frequency. The loss tangent is defined as the ratio of the energy lost to the energy stored, which is the ratio of the imaginary part of the permittivity to the real part:

$$\tan\delta = \frac{\varepsilon_r''}{\varepsilon_r'}$$

For RF propagation modeling, the real and imaginary parts of the relative permittivity (and therefore the loss tangent) are essential parameters. Dielectric impedance measurement or dielectric spectroscopy is the process of measuring these electrical properties of materials over a range of frequencies.

The Stevens HydraProbe [5] (shown in Figure 3) is a commercially available soil sensor used for the measurement of soil moisture, electrical conductivity, and temperature. The device is typically used for measuring the dielectric properties of soil for agricultural applications, which can then be used to provide information about the soil moisture content, salinity, and other related properties. The

HydraProbe is primarily intended for determining the moisture content in soils by measuring the complex permittivity. For the temperature, a thermistor inside of the probe head is utilized. The device applies the method of coaxial impedance dielectric reflectometry. The system is fed by a planar waveguide and consists of four electrodes or probes that are inserted into the soil. These probes act in concert to form a coaxial transmission line and are used to apply an electrical signal to the soil and measure the response. Measurements of the real and imaginary parts of the complex relative permittivity, ε_r (ε_r' and ε_r'', respectively), are calculated for a frequency of 50 MHz. By analyzing the phase and amplitude of the signal as it travels through the soil and the interactions with soil particles and moisture, the device can calculate the soil dielectric constant. The accuracy and precision of the HyrdraProbe according to the manufacturer's specifications [5] are provided in Table 2.

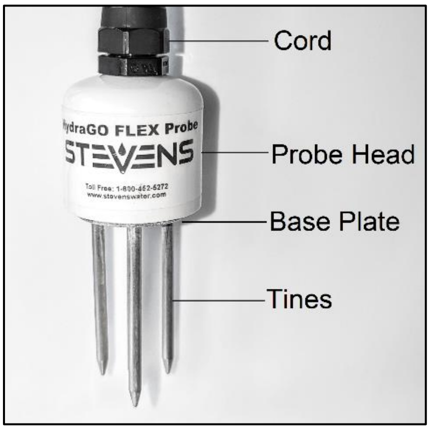

Figure 2: A diagram of the HydraProbe used for data acquisition

Table 2: Stevens HydraProbe Accuracy and Precision [5]

Parameter	Accuracy/Precision
Real Dielectric Permittivity (isolated)	-Range: 1 to 80 where 1 = air, 80 = Distilled Water -Accuracy: < ± 0.5% Or ± 0.25 dielectric units
Imaginary Permittivity	-Range: 0 to 80 -Accuracy: ± 0.1 up to 0.25 S/m and ± 7 at or above 0.5 S/m
Soil Moisture for Inorganic Mineral Soils	-Range: completely dry to Full saturation -Accuracy: ±0.01 WFV for most soils (θ m^3, m^{-3}) ± ≤0.03 for fine textured soils
Bulk Electrical Conductivity	-Accuracy: ±2.0% or 0.02 S/m (whichever is greater) -Range: 0 to 1.5 S/m
Temperature	Accuracy: ±0.3°C Range: -10 to 60°C

The simulant was contained in a cylindrical 400ml Pyrex beaker for all measurements. Preparation of the simulant and subsequent measurements were conducted inside of a fume hood to preclude any exposure to fine particulate. Between successive measurements, the contents were baked at a temperature of 130°C for a minimum of 2.5 hours. The intent of this baking process was to purge the simulant of water that may have diffused into the system under ambient conditions. The HydraProbe was then inserted into the center of the simulant until the base plate was flush with the surface. Given that the internal thermistor of the HydraProbe is embedded in the base plate, this model of the sensor requires full system temperature equilibration before accurate temperature measurements can be taken. For additional temperature measurement of the simulant, the tip of a type K thermocouple was also buried halfway down into the simulant at approximately 2/3 the radius of the container from the center. This thermocouple has a standard error that is the greater of 2.2 K or 0.75% [6]. For room temperature measurements (roughly 22-25°C), the vessel was also sealed to minimize introduction of moisture from the ambient environment.

Measurements made on the relative effects on permittivity due to moisture were also completed. First, a tube was inserted into the vessel for the purpose of later introducing deionized water to the base of the dried simulant. The dried simulant was then added into the container for measurement and the

HydraProbe was inserted in same manner as above. It should be noted that all moisture measurements were made in the room temperature range and that water was added gently in increments of approximately 10 milliliters. Care was taken to avoid excessive force which could lead to compaction and granule displacement at the base of the beaker. Following the polynomial curve fitting calibration, using the Topp equation [7] (below), a polynomial fit of ε_r' from soil moisture content was calibrated for the sensor. Where θ is the moisture volume fraction:

$$\theta = A + B\varepsilon_r' + C{\varepsilon_r'}^2 + D{\varepsilon_r'}^3$$

For the temperature sweep, the sample was first moved from 130°C to 87°C. The intention was to slowly cool the sample towards the maximum target testing temperature of the probe (60°C) without exposure to ambient conditions to avoid implicit moisture contamination. Measurements were then taken at quasi-regular intervals until the sample temperature leveled off to ambient.

Results

For dry simulant at ambient temperature, the results are provided in Table 3. The mean values presented are computed from 46 individual measurements. The HydraProbe precision for the real dielectric constant is listed as 0.1. Considering that the HydraProbe is designed for measurement of soil samples in which the imaginary permittivity component is dominated by the moisture content, the imaginary part of the permittivity for a dry regolith sample is expected to be below the measurement sensitivity at +/- 0.1 of full scale. As a result, the measurement for the imaginary component, and hence the loss tangent, is expected to be limited by the capabilities of the measurement hardware.

Table 3: Measurement results for dry simulant at room temperature

Parameter	Mean	Standard Deviation
Temperature (°C)	23.84	0.089
Soil Moisture (%)	0.16	0.376
Real Permittivity ε_r'	2.75	0.115
Imaginary Permittivity ε_r''	0.13	0.047
Loss Tangent [tan δ]	0.047	0.015

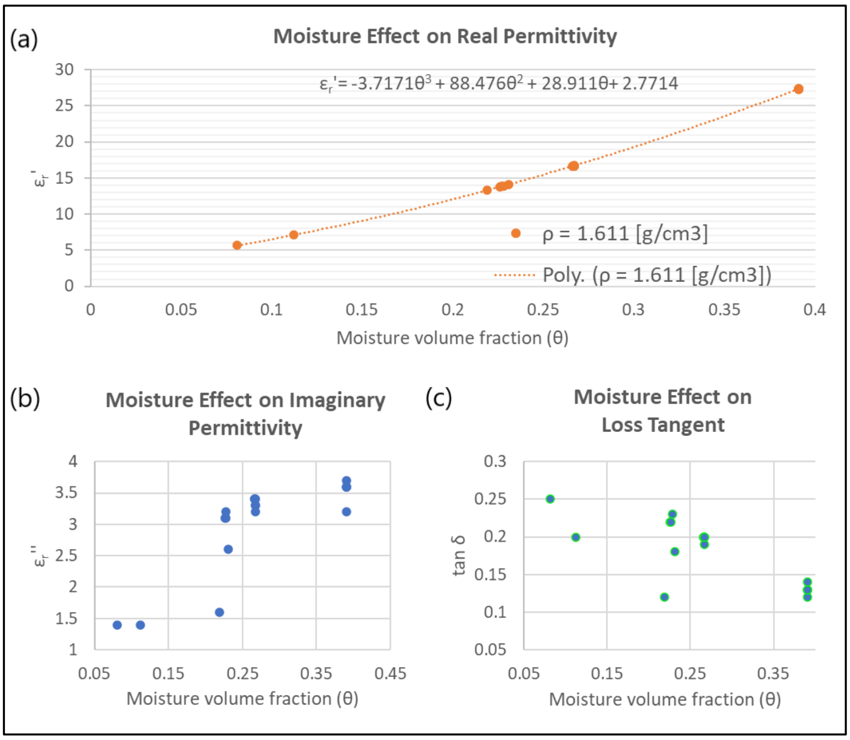

Figure 3: Plots of (a) real permittivity, (b) imaginary permittivity, and (c) loss tangent of the simulant as a function of moisture level.

Moisture measurements of the simulant, summarized in Figure 3 (above), demonstrate the predicted relationship between the water concentration and permittivity, previously shown by Topp et. al [7]. The third-order polynomial curve fit follows the Topp equation and maintains a zeroth-order term like the value for simulant real permittivity in ambient conditions (Figure 3a). The following equation is the direct Topp equation, solved for theta:

$$\theta = (9 \times 10^{-6})(\varepsilon_r')^3 - 0.0007(\varepsilon_r')^2 + 0.0287\varepsilon_r' - 0.0611$$

Furthermore, an essentially linear relationship between moisture and the imaginary component of the complex permittivity is observed (Figure 3b). As expected, with the increase in water content, the loss tangent begins to exhibit behavior heavily affected by the imaginary permittivity (Figure 3c).

For the temperature sweep, as may be expected, the real part of the permittivity trends in a positive manner as temperature increases (Figure 4). Given the constraints of the probe design, a thoroughly dried simulant did not offer a stable set of values of the imaginary permittivity or loss tangent within the resolution of the device (± 0.1). However, the value near room temperature for ε_r' is within range of the expectation from the room temperature results.

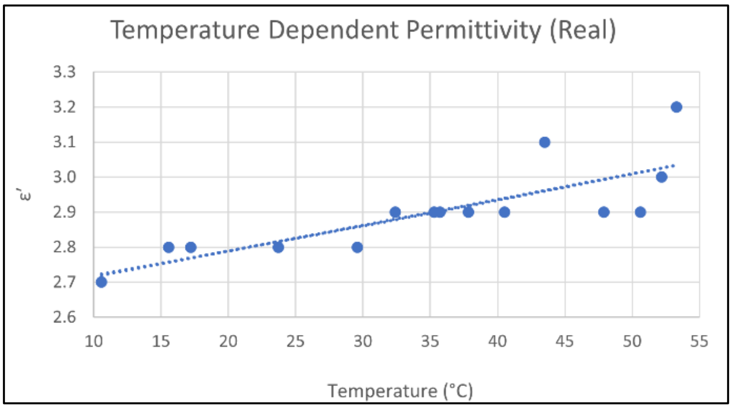

Figure 4: The real permittivity of the simulant as function of temperature.

Discussion

The Maxwell Garnett equation is utilized as an approximation for the effective permittivity, ε_{eff}, of a given heterogenous medium [8]. The volume fraction contributed by each species in a mixed system influences the effective permittivity in a proportional manner. For the case of the simulant, a multiphase mixture (those that include more than one 'inclusion' constituent with an associated permittivity in a prevailing environmental species with a permittivity of its own), the equation takes the following form if spheroid particles are assumed

$$\varepsilon_{eff} = \varepsilon_e + 3\varepsilon_e \frac{\sum_{k=1}^{k} f_k \frac{\varepsilon_k - \varepsilon_e}{\varepsilon_k + 2\varepsilon_e}}{1 - \sum_{k=1}^{k} f_k \frac{\varepsilon_k - \varepsilon_e}{\varepsilon_k + 2\varepsilon_e}}$$

where ε_k is the permittivity of the k-th component, f_k is the volume fractional percent and ε_e is the permittivity of the surrounding medium, which in this case is assumed to be air. The fractional percentage and corresponding permittivity for each of the components in the NU-LHT-2M (NASA/USGS-Lunar Highlands type) simulant is given in table 4.

Table 4: Permittivity of NU-LHT-2M components and corresponding fractional percents

	SiO_2	Al_2O_3	CaO	MgO	FeO	Na_2O
ε_r	3.9 [9]	9-10 [10]	11.95 [11]	9.1-11.2 [12]–[14]	~25 [15], [16]	7.57 [17]
f	47.93	24.57	13.2	8.55	4.33	1.41

Olhoeft and Strangway [18] suggested the fit of the complex relative permittivity to the expression $\varepsilon_r' = A^{\rho}$. Subsequent publications have proposed the lunar regolith follows the expression with A = 1.919

[19]–[21]. For the lunar simulants, Barmatz et al. 2023 indicated a value of A = 2.11 (for measurements near 2.45 GHz at room temperature) and provided a second order fit to all the simulants tested [22]:

$$\varepsilon_r' = 0.9334 + 0.91\rho + 0.3621\rho^2$$

The second order polynomial fit provided by Barmatz indicates that when the density of the simulant approaches zero, the relative permittivity approaches the provided constant of 0.9334. The corresponding physics suggests that when the simulant density approaches zero, the permittivity would approach that of vacuum and hence the relative permittivity would approach unity. A relative permittivity of unity for a density approaching zero is consistent with the expression suggested by Olhoeft and Strangway [18]. Using the data published in Barmatz ([22], Table 1), a second order polynomial is fit to the data, where the intercept value is constrained to unity. The data and universal polynomial fit are shown in figure 5a, where the polynomial fit to the published data is given by:

$$\varepsilon_r' = 1.0 + 0.835\rho + 0.3761\rho^2$$

Figure 5b plots the various models as a function of density and table 5 lists the value of the permittivity calculated by each of the various model results using the NU-LHT-2M density as measured in this work. It should be noted that the curve fit to the data published in Barmatz [22]is the result of a universal fit to all the published simulant measurements. Barmatz [22] indicates a plasma processed version of the NU-LHT-2M (no nFe) was measured with ε_r' =2.794, which is consistent with the measurements in this work. The values associated with the universal simulant curve fit yield higher values (ε_r'=3.3) than the curve fit to the Apollo regolith (ε_r'=2.8) and similarly to the result of the Maxwell-Garnett equation (ε_r'= 2.9).

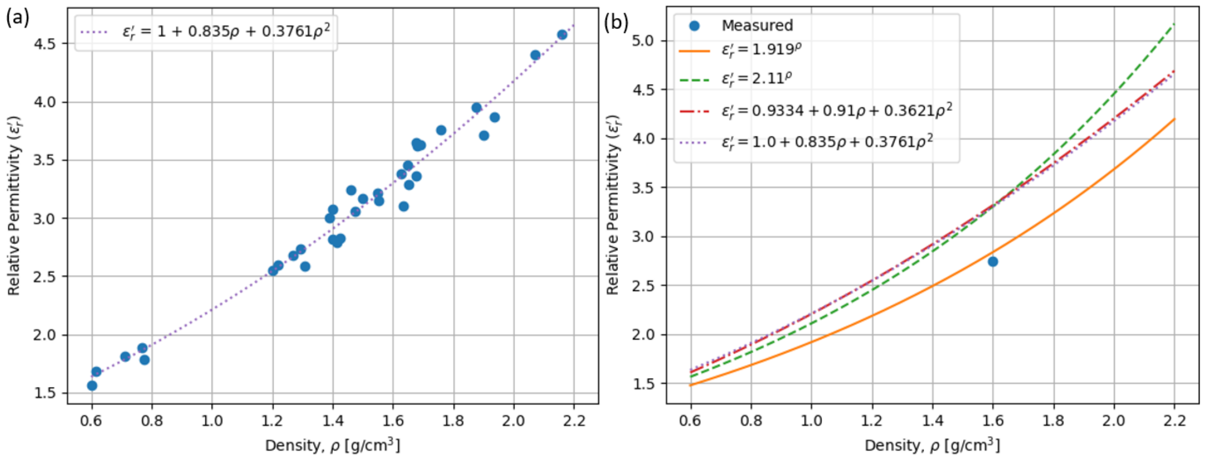

Figure 5: (a) (left) Curve fit to Barmatz 2023 lunar simulant data [22] with curve fit intercept value of one. (b) (right) Relative permittivity models as a function of density. The value of the relative permittivity as measured by the probe in this work is depicted as the "Measured" value.

Table 5: Modeled relative permittivity compared to measured value using ρ = 1.598 g/cm^3

	Measurement	Maxwell-Garnett	$\varepsilon_r' = A^\rho$		$\varepsilon_r' = c + b\rho + a\rho^2$	
Parameters	HydraProbe	Table 4	A = 1.919	A = 2.11	c = 0.9334 b = 0.91 a = 0.3621	c = 1.0 b = 0.835 a = 0.3761
Permittivity ε_r'	2.75 std=0.115	2.920	2.833	3.298	3.312	3.295
Modeled Material	NU-LHT-2M	NU-LHT-2M	Apollo Regolith	Multiple Simulants	Multiple Simulants	Multiple Simulants

The measurement results are not expected to accurately represent the loss tangent due to measurement range and resolution. The model of the loss tangent for the lunar highlands regolith as a function of density is given as [23]:

$$\tan\delta = \frac{\varepsilon_r''}{\varepsilon_r'} = 10^{\left(0.312\rho + f^{0.069} - 3.79\right)}$$

where the frequency *f* is in GHz. The corresponding loss tangent for a density of 1.598 g/cm^3 corresponds to $\tan\delta$ = 3.32e-3, which corresponds to an imaginary component of the relative permittivity $\varepsilon_r'' = \varepsilon_r' \tan\delta$ = 3.32e-3 * 2.83 = 9.39e-3. Thus, the expected value for the loss tangent is below the measurement sensitivity for the HydraProbe hardware.

The HydraProbe soil sensor is designed for measurement of soil properties, where the sensor may be buried below the surface at depths of 5 cm to 2 m deep. Temperature sensor measurements inside the probe rely on the system reaching thermal equilibrium. During the experiment, the HydraProbe sensor was not submerged in the regolith simulant, but rather was placed on the surface with the tines penetrating the simulant. The observed temperature measurements as reported by the HydraProbe did not match the values reported by the thermocouple. The simulant was approximately 60°C sometime after being removed from the oven, and the HydraProbe sensor probes (at room temperature) were then inserted into the simulant. Due to the thermal capacitance of the HydraProbe sensor, the dynamic temperature change of the simulant was not accurately measured by the HydraProbe. Fortunately, given the dry, low salinity conditions of the simulant, there was little expected augmentation from moisture or electrical conductivity changes as a function of temperature. Temperature dependent error to the measured electrical parameters from the device are expected to have minimal impact on experimental data due to the device applying temperature correction parameters to measurements with low values of moisture and electrical conductivity.

Conclusions & Future Work

A commercially available soil sensor was used for the measurement of the complex relative permittivity of the NASA/USGS-Lunar Highlands regolith simulant NU-LHT-2M. While the measurement results for the imaginary component of the complex relative permittivity are below the resolution of the device for a dry sample, the real component measurements agree with values as published in the literature. Results for the simulant in the presence of moisture are also provided. The measurements of the moist samples align with the anticipated trend for water presence in the material. Future work should include advancements in dielectric modeling. Some additional attention may include but not ultimately be limited to chemical alterations, particle size distribution, and grain elongation.

In keeping with the developmental aims of characterizing all pertinent frequencies, future work will continue to investigate simulants perhaps eventually South Pole regolith samples in bands of interest. In the near term, the waveguide transmission line technique will be used to assess NU-LHT-2M at K-band (18 – 27 GHz), Ka-band (27 – 40 GHz), and potentially X-band (~7-12 GHz), which covers the bands expected to provide high-rate return links for lunar missions. Experimental variables will again consider moisture content and temperature, including ranges down to the cryogenic temperatures of the lunar night. Supplemental measurements at UHF and S-bands may also be conducted using capacitive and cavity resonant methods to validate previous results. Additionally, the HydraProbe, a commercial product already validated for broad soil analysis and reporting, may provide additional utility as a valuable field tool for characterizing soils during terrestrial field testing of moon-bound wireless communications systems.

References

[1] V. L. Prabhu, “Microwave heating of lunar simulants JSC-1A and NU-LHT-3M: experimental and theoretical analysis”.

[2] Space Frequency Coordination Group, “Recommendation SFCG 32-2R5: Communication and positioning, navigation, and timing frequency allocations and sharing in the lunar region.” 2023. [Online]. Available: https://www.sfcgonline.org/Resources/Recommendations/default.aspx

[3] D. Stoeser, D. Rickman, and S. Wilson, “Design and Specifications for the Highland Regolith Prototype Simulants NU-LHT-1M and -2M,” 2010. Accessed: Sep. 20, 2023. [Online]. Available:

https://www.semanticscholar.org/paper/Design-and-Specifications-for-the-Highland-Regolith-Stoeser-Rickman/5d64100053c55e44a79734d167e9d6393963d8a9

[4] X. Zeng, C. He, and A. Wilkinson, “Geotechnical Properties of NT-LHT-2M Lunar Highland Simulant,” *J. Aerosp. Eng.*, vol. 23, no. 4, pp. 213–218, Oct. 2010, doi: 10.1061/(ASCE)AS.1943-5525.0000026.

[5] Stevens, “Hydroprobe Manuel.” 2018. [Online]. Available: https://stevenswater.com/resources/documentation/hydraprobe/HydraProbe_Manual_Jan_2018.pdf

[6] “What is a type K Thermocouple?,” *https://www.omega.com/en-us/*. https://www.omega.com/en-us/resources/k-type-thermocouples (accessed Sep. 19, 2023).

[7] G. C. Topp, J. L. Davis, and A. P. Annan, “Electromagnetic determination of soil water content: Measurements in coaxial transmission lines,” *Water Resour. Res.*, vol. 16, no. 3, pp. 574–582, 1980, doi: 10.1029/WR016i003p00574.

[8] A. Sihvola, *Electromagnetic Mixing Formulas and Applications*. IET Digital Library, 1999. doi: 10.1049/PBEW047E.

[9] P. Zukowski, T. N. Koltunowicz, K. Czarnacka, A. K. Fedotov, and I. E. Tyschenko, “Carrier transport and dielectric permittivity of SiO2 films containing ion-beam synthesized InSb nanocrystals,” *J. Alloys Compd.*, vol. 846, p. 156482, Dec. 2020, doi: 10.1016/j.jallcom.2020.156482.

[10] S. J. Penn *et al.*, “Effect of Porosity and Grain Size on the Microwave Dielectric Properties of Sintered Alumina,” *J. Am. Ceram. Soc.*, vol. 80, no. 7, pp. 1885–1888, Jan. 2005, doi: 10.1111/j.1151-2916.1997.tb03066.x.

[11] M. A. Subramanian, R. D. Shannon, B. H. T. Chai, M. M. Abraham, and M. C. Wintersgill, “Dielectric constants of BeO, MgO, and CaO using the two-terminal method,” *Phys. Chem. Miner.*, vol. 16, no. 8, pp. 741–746, Nov. 1989, doi: 10.1007/BF00209695.

[12] H. Kassem *et al.*, “LaTiOxNy Thin Films, Measurement and Application to Microwave Device,” *2008 38th Eur. Microw. Conf.*, pp. 1362–1365, Oct. 2008, doi: 10.1109/EUMC.2008.4751717.

[13] J. D. Hwang and C.-Y. Chang, “Post-annealing treatment in improving high dielectric constant MgO-based metal-oxide-semiconductor diodes,” *Appl. Phys. Lett.*, vol. 120, no. 25, p. 252902, Jun. 2022, doi: 10.1063/5.0094513.

[14] S. Lee *et al.*, “Enhanced dielectric properties of Be-doped magnesium oxide nanopowder,” *AIP Adv.*, vol. 13, no. 1, p. 015007, Jan. 2023, doi: 10.1063/5.0130595.

[15] *Non-Tetrahedrally Bonded Binary Compounds II*. Accessed: Sep. 20, 2023. [Online]. Available: https://link.springer.com/book/9783540649663

[16] L.-S. Fu, J.-T. Jiang, C.-Y. Xu, and L. Zhen, “Synthesis of hexagonal Fe microflakes with excellent microwave absorption performance,” *CrystEngComm*, vol. 14, no. 20, pp. 6827–6832, Sep. 2012, doi: 10.1039/C2CE25836F.

[17] I. Petousis *et al.*, “High-throughput screening of inorganic compounds for the discovery of novel dielectric and optical materials,” *Sci. Data*, vol. 4, no. 1, Art. no. 1, Jan. 2017, doi: 10.1038/sdata.2016.134.

[18] G. R. Olhoeft and D. W. Strangway, “Dielectric properties of the first 100 meters of the Moon,” *Earth Planet. Sci. Lett.*, vol. 24, no. 3, pp. 394–404, Jan. 1975, doi: 10.1016/0012-821X(75)90146-6.

[19] W. D. Carrier III, G. R. Olhoeft, and W. Mendell, *Physical Properties of the Lunar Surface*. 1991, pp. 475–594. Accessed: Sep. 20, 2023. [Online]. Available: https://ui.adsabs.harvard.edu/abs/1991lsug.book..475C

[20] J. Lai, Y. Xu, X. Zhang, and Z. Tang, “Structural analysis of lunar subsurface with Chang׳E-3 lunar penetrating radar,” *Planet. Space Sci.*, vol. 120, pp. 96–102, Jan. 2016, doi: 10.1016/j.pss.2015.10.014.

[21] J. Feng, Y. Su, C. Ding, S. Xing, S. Dai, and Y. Zou, “Dielectric properties estimation of the lunar regolith at CE-3 landing site using lunar penetrating radar data,” *Icarus*, vol. 284, pp. 424–430, Mar. 2017, doi: 10.1016/j.icarus.2016.12.005.

[22] M. Barmatz, D. Steinfeld, J. Batres, H.-Y. Hao, D. Rickman, and H. Shulman, “Microwave permittivity and permeability measurements on lunar simulants at low temperatures,” *Adv. Space Res.*, Aug. 2023, doi: 10.1016/j.asr.2023.08.041.

[23] M. A. Siegler, J. Feng, P. G. Lucey, R. R. Ghent, P. O. Hayne, and M. N. White, “Lunar Titanium and Frequency-Dependent Microwave Loss Tangent as Constrained by the Chang’E-2 MRM and LRO Diviner Lunar Radiometers,” *J. Geophys. Res. Planets*, vol. 125, no. 9, p. e2020JE006405, 2020, doi: 10.1029/2020JE006405.